Geophysical Research Letters®

RESEARCH LETTER
10.1029/2021GL094305

Key Points:

- A complex hillslope dynamics is associated with the linear to nonlinear sediment flux transition
- Hillslopes filtering potential of external signals is highly contrasted depending on the type of forcing
- Changes in the climatic signal frequency at the Mid-Pleistocene Transition could induce a significant shift in hillslope erosional response

Supporting Information:

Supporting Information may be found in the online version of this article.

Correspondence to:

V. Godard,
godard@cerege.fr

Citation:

Godard, V., & Tucker, G. E. (2021). Influence of climate-forcing frequency on hillslope response. *Geophysical Research Letters*, *48*, e2021GL094305. https://doi.org/10.1029/2021GL094305

Received 14 MAY 2021
Accepted 18 AUG 2021

Influence of Climate-Forcing Frequency on Hillslope Response

V. Godard[1,2] and G. E. Tucker[3,4]

[1]CNRS, IRD, INRAE, Coll France, CEREGE, Aix-Marseille University, Aix-en-Provence, France, [2]Institut Universitaire de France (IUF), Paris, France, [3]Cooperative Institute for Research in Environmental Sciences (CIRES), University of Colorado, Boulder, CO, USA, [4]Department of Geological Sciences, University of Colorado, Boulder, CO, USA

Abstract Assessing rivers' and hillslopes' sensitivity to external forcing is paramount to understand landscape evolution, in particular as a response to Quaternary climate changes. River networks are usually considered to be the main conveyors of environmental signals, such as changes in precipitation, temperature, or baselevel. Yet because hillslopes provide the source of sediment for river networks, their response to environmental change also modulates landscape dynamics. In order to characterize such behavior, we analyze the response times of a transport-limited hillslope. We use simple numerical models of denudation to study hillslope responses to oscillatory forcing and understand their filtering effects on environmental signals. Modifications in the frequency of climate oscillation, such as the change that occurred at the Mid-Pleistocene Transition, can significantly modulate hillslope sediment-flux response. We infer a wide range of hillslope responses, ranging from negligible change over the full range of climate-forcing frequencies, to a significant filtering of long-period signals.

Plain Language Summary Landscapes are constituted of hillslopes and rivers where different types of erosion and sediment transport processes take place. Due to their large extent, river networks are an important driver of global landscape response to climatic or tectonic changes. Hillslopes have smaller dimensions but are also where most sediment production occurs and for that reason it is important to have a good understanding of how they respond to perturbations. We use simple numerical models of hillslope evolution to study the influence of oscillating changes of either the efficiency of sediment transport across the hillslope or the rate of channel downcutting at its base. Our results indicates that the period of oscillations for these perturbations controls the amplitude of the sediment flux response out of the hillslope, and provide a framework to understand how this landscape component reacts to climatic cycles such as the glacial/inter-glacial oscillations of the Quaternary. For example, a major change occurred 800 ka ago with a shift in climate oscillation from 40 to 100 ka period. Our models suggest that in some landscapes this change in period alone could have induced a significant decrease in the amplitude of hillslope sediment flux response.

1. Introduction

Landscapes evolve in response to changes in their climatic and tectonic boundary conditions. River networks are usually considered to be the main agents that transmit the effects of such external forcing across landscapes. Due to their dominance in terms of area covered at the Earth's surface, most weathering and sediment production occurs on hillslopes. Geomorphologists sometimes assume that the erosion rate on hillslopes closely follows the pace imposed by channel downcutting at their feet (e.g., Ouimet et al., 2009). However, several studies have highlighted the potential for a more complex behavior of hillslopes, suggesting that landscape response depends on the nature of the coupling between channels and hillslopes and on the intrinsic dynamics of hillslopes and their response timescales (e.g., Clubb et al., 2020; Langston et al., 2015; Romans et al., 2016; Watkins et al., 2018). The hypothesis that hillslope sediment flux depends linearly on topographic gradient, which underpins the diffusion theory of soil-mantled hillslope evolution, has provided a simple and robust framework for understanding their behavior (Culling, 1960; Gilbert, 1909). However, a growing body of evidence points to a nonlinear relationship between sediment flux and hillslope gradient (Andrews & Bucknam, 1987; Doane et al., 2018; Furbish & Roering, 2013; Roering et al., 1999; Tucker & Bradley, 2010), which complicates the hillslope response to external forcing and its relationship with the fluvial network. Forcing factors acting on landscapes can be classified into two broad

categories (Mudd, 2016). Climate acts directly as a Top-Down (TD) forcing, producing changes in surface runoff and vegetation cover, which modulate sediment transport efficiency along hillslopes. Bottom-Up (BU) forcing, resulting from changes in the baselevel fall rate at the toe of the hillslope, is associated with incision or aggradation in the channel, and can be controlled by any factor impacting the baselevel, such as climate, tectonics, eustatic variations, or auto-cyclic processes.

The response time of hillslopes has been intensively studied and characterized under these various types of forcing (Fernandes & Dietrich, 1997; Roering et al., 2001). It is less clear how this response time interacts with the time characteristics of the input forcing, in particular when dealing with periodic signals associated with climatic variability. Several recent studies focusing on the fluvial domain have highlighted the sensitivity to periodic climatic fluctuations and the importance of their frequency content (Braun et al., 2015; Godard et al., 2013; Simpson & Castelltort, 2012). The response of the hillslope domain to such forcing has received less attention. Diffusive processes are usually considered to have a strong buffering effect on environmental signals (e.g., Godard et al., 2013), but the signature of more complex hillslope behavior remains to be clearly characterized. From gently rolling hillslopes in low-relief landscapes to near-threshold slopes in actively uplifting areas, hillslopes can present a variety of morphologies, and understanding their importance for landscape evolution requires assessing which types of hillslopes, characterized by a given relief or erosion regime, are most sensitive to the different types of forcing factors.

Here, we study the response of hillslopes to periodic variations in climatic and tectonic (baselevel) boundary conditions, with a specific focus on the implication of the nonlinear relationship between sediment flux and gradient. We summarize the existing framework used to formulate hillslope evolution, and its relationship with response time and topographic metrics. We then assess the controls of baselevel fall (here "uplift") rate and transport coefficient on hillslope response. We specifically study the relationship between the forcing period and the response time of hillslopes, as set by length, uplift rate, and transport efficiency, and discuss the implications for landscape dynamics.

2. Theoretical Background

We present here the theoretical formulation for hillslope erosion and sediment flux, and the modeling approaches used in this study. Mass conservation applied to 1D hillslope evolution can be expressed as,

$$\frac{\partial z}{\partial t} + \frac{\partial q}{\partial x} = \beta U, \tag{1}$$

where z is land surface elevation, t time, q sediment flux ($[L^2T^{-1}]$), β the rock-to-regolith density ratio, and U the rate of rock uplift relative to baselevel at the foot of the hillslope ($[LT^{-1}]$). Equation 1 can be combined with a Geomorphic Transport Law (GTL, Dietrich et al., 2003), describing sediment flux q over a hillslope. A widely used transport law for soil-mantled hillslopes (Roering et al., 1999, 2007) expresses the flux q as a nonlinear function of local slope gradient,

$$q = \frac{-K(\partial z \,/\, \partial x)}{1 - \left[(\partial z \,/\, \partial x) \,/\, S_c\right]^2}, \tag{2}$$

where K is a transport coefficient ($[L^2T^{-1}]$) and S_c a critical hillslope gradient ($[L\,/\,L]$) (Roering et al., 1999). This expression applies only for $|\partial z\,/\,\partial x| < S_c$. The transport law (Equation 2) implies that the degree of nonlinearity in the relationship between gradient and sediment flux varies with the gradient itself. For our analysis, it is useful to quantify this degree of nonlinearity by separating the total flux into linear and nonlinear components. Doing so starts with the observation that in gently sloping parts of the landscape, such as areas close to the hilltops, the sediment flux is linearly related to topographic gradient as $q_l = -K\partial z\,/\,\partial x$. As shown by Roering et al. (2001), the total flux q can be expressed as the sum of a linear q_l and a nonlinear q_{nl} component,

$$q = q_l + q_{nl} = K\frac{\partial z}{\partial x} + \frac{K\frac{\partial z}{\partial x}\left(\frac{\partial z\,/\,\partial x}{S_c}\right)^2}{1-\left(\frac{\partial z\,/\,\partial x}{S_c}\right)^2}. \tag{3}$$

Substituting Equation 2 into Equation 1 yields a landscape evolution model describing the evolution of hillslope profile topography $z(x,t)$ through space and time,

$$\frac{\partial z}{\partial t} - K\frac{\partial^2 z}{\partial x^2}\frac{1+\left(\frac{\partial z\,/\,\partial x}{S_c}\right)^2}{\left(1-\left(\frac{\partial z\,/\,\partial x}{S_c}\right)^2\right)^2} = \beta U. \tag{4}$$

We solve Equation 4 using the implicit method proposed by Perron (2011). Starting from a steady-state topography we submit the hillslope to time variations in either K or U, parameterized with sinusoidal functions,

$$K(t) = K_0\left(1 + a\sin\left(\frac{2\pi t}{T}\right)\right), \quad U(t) = U_0\left(1 + a\sin\left(\frac{2\pi t}{T}\right)\right). \tag{5}$$

K_0 and U_0 are the average values of K and U, respectively, a is a factor controlling the amplitude of the forcing, and T is the oscillation period. The reference parameter values used in our simulations are listed in Table S1.

Under steady conditions ($\partial z/\partial t = 0$), Equation 4 can be integrated to yield the steady-state topographic profile (Roering et al., 2001),

$$z(x) = \frac{KS_c^2}{2\beta U}\left(\ln\left(\frac{1}{2}\sqrt{1+\left(\frac{2\beta U x}{KS_c}\right)^2} + \frac{1}{2}\right) - \sqrt{1+\left(\frac{2\beta U x}{KS_c}\right)^2} + 1\right), \tag{6}$$

with L as the hillslope length (horizontal distance from hilltop to channel). It is useful to define a reference erosion rate (Roering et al., 2007) as,

$$E_R = \frac{KS_c}{2L\beta}, \tag{7}$$

This reference value provides a way to normalize steady-state erosion rate $E = U$ into its non-dimensional equivalent as,

$$E^* = \frac{2L\beta U}{KS_c}. \tag{8}$$

At steady state, and in the vicinity of hilltops, where topographic gradient is small ($\partial z/\partial x \ll S_c$), Equation 4 simplifies to,

$$U = -\frac{KC_{HT}}{\beta}, \tag{9}$$

where hilltop curvature C_{HT} is the second derivative of topography. Combining Equations 8 and 9 yields a form of E^* that can be calculated directly from topographic data without needing to know K (Hurst et al., 2012; Roering et al., 2007),

$$E^* = \frac{2C_{HT}L}{S_c}. \tag{10}$$

In order to assess the relative non-linear contribution to the sediment flux, Roering et al. (2001) introduced the ratio Ψ of the two components,

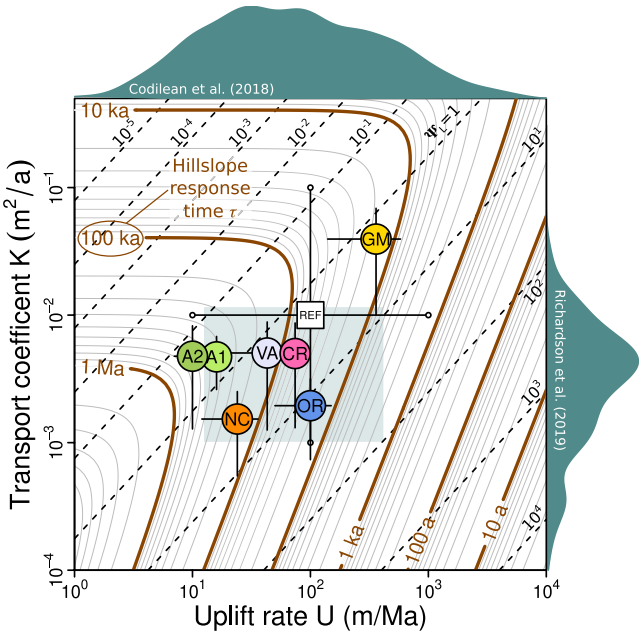

Figure 1. Hillslope response timescale τ (solid contours) (Roering et al., 2001) as a function of transport coefficient K and uplift rate U. Dashed lines correspond to different values of the nonlinear transport ratio Ψ_L (Roering et al., 2001). Kernel Density Estimates for transport coefficient (Richardson et al., 2019) and erosion rate (Codilean et al., 2018) compilations are also plotted in front of the corresponding axes. The light blue rectangle indicates the interquartile range from both data sets. Black-bordered white square shows the reference K and U values, while small white circles indicate other pairs of values tested in Figure 3. Colored circles correspond to the case studies presented in the supplementary materials (Table S2). A1 and A2: Southeastern Australian Escarpment, lowlands and highlands, respectively (Godard et al., 2019). CR: Cascade ridge, Sierra Nevada, CA (Grieve et al., 2016; Hurst et al., 2012). GM: Gabilan Mesa, CA (Grieve et al., 2016; Roering et al., 2007). NC: Coweeta, southern Appalachians, NC (Grieve et al., 2016). OR: Oregon Coast Range, OR (Grieve et al., 2016; Roering et al., 2007). VA: Valensole Plateau, Provence, France (Godard et al., 2020).

$$\Psi = \frac{q_{nl}}{q_l} = \frac{\left(\frac{\partial z / \partial x}{S_c}\right)^2}{1 - \left(\frac{\partial z / \partial x}{S_c}\right)^2}. \tag{11}$$

Following Roering et al. (2001), and using Equation 6, we evaluate this ratio at the base of the hillslope,

$$\Psi_L = \Psi(x = L) = \frac{\left(\frac{S_c}{2\beta UL}\left(-K + \sqrt{K^2 + \left(\frac{2\beta UL}{S_c}\right)^2}\right)\right)^2}{1 - \left(\frac{S_c}{2\beta UL}\left(-K + \sqrt{K^2 + \left(\frac{2\beta UL}{S_c}\right)^2}\right)\right)^2}, \tag{12}$$

and we use their definition of an exponential equilibrium adjustment timescale for sediment flux or hillslope morphology calculated as,

$$\tau = \frac{AL^2}{K(1 + \Psi_L)^B}. \tag{13}$$

The parameters $A = 0.405$ and $B = 1.74$ were calibrated by Roering et al. (2001) over a range of Ψ_L values reflecting a wide range of environmental conditions and using numerical models for hillslope evolution based on the same physical principles as the one we use here. Substituting Equation 8 into Equation 12 yields,

$$\Psi_L = \frac{1}{2}\sqrt{1 + E^{*2}} - \frac{1}{2} \tag{14}$$

The non-dimensional framework for hillslope morphology analysis introduced by Roering et al. (2007) provides a way to reduce erosion dynamics to non-dimensional erosion rates E^* (Equation 8), which can be computed on the basis of measurable hillslope morphological characteristics (Equation 10), such as length and hilltop curvature (Grieve et al., 2016). Equation 14 describes the connection between E^*, which can be measured from topographic data, and the degree of nonlinearity of the sediment flux (Ψ_L). In order to compare theoretical predictions of hillslope behavior with actual landscapes, we select case studies for which landscape denudation rates have been constrained with terrestrial cosmogenic nuclides, and where hillslope-scale morphological properties such as hilltop curvature C_{HT} and hillslope length L have been determined with methods similar to those proposed by Hurst et al. (2012) and Grieve et al. (2016) using high resolution topographic data (Figure 1 and Table S2). The topographic data enable calculation of E^* for these sites (Equation 10), and the cosmogenic data constrain the value of the baselevel parameter U. We also use the global compilations of hillslope transport coefficients by Richardson et al. (2019) and denudation rates by Codilean et al. (2018) to put the inferred hillslope behavior into a broader context.

3. Results

3.1. Controls on Response Time

Low values (<0.1) of the nonlinear transport ratio Ψ_L (Equation 12) correspond to hillslopes in the linear regime (Figure 1), where response times are insensitive to changes in uplift rate and larger than 100 ka, for observed values of the transport coefficient (Richardson et al., 2019). Conversely, high Ψ_L values (>1) are associated with dominant contributions of nonlinear fluxes, a situation where response times are controlled by both transport coefficient and uplift rate and where response times are less than 100 ka, expect

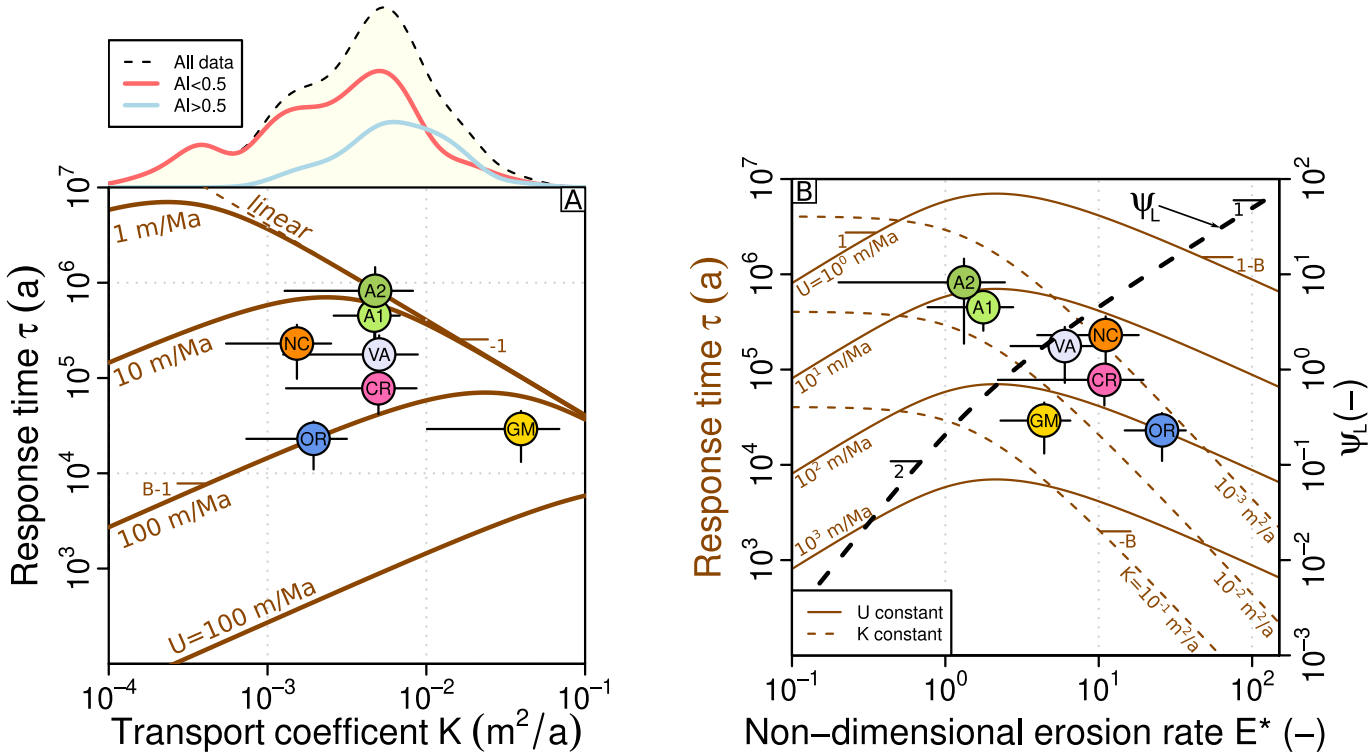

Figure 2. (a) Evolution of response timescale τ (Roering et al., 2001) as a function of transport coefficient K, for different values of uplift rate U. Brown dashed line corresponds to purely linear diffusion ($\Psi_L = 0$ in Equation 13). Kernel Density Estimates for transport coefficients compiled by Richardson et al. (2019) are also plotted above the graph. Black dashed line is the whole data set, whereas red and blue lines correspond to Aridity Index (AI) lower or higher than 0.5, respectively. Colored circles correspond to the case studies presented in the text and on Figure 1. Reported slope values correspond to the exponents of asymptotic power law relationships between τ and K. (b) Evolution of hillslope response time τ as a function of non-dimensional erosion rate E^* (Roering et al., 2007), for different constant transport coefficient K (dashed brown lines) or uplift rates U (solid brown lines) values. Dashed black line shows the evolution of the nonlinear transport ratio Ψ_L (Roering et al., 2001) as a function of non-dimensional erosion rate E^*. Colored circles correspond to the case studies presented in Figure 1 and supplementary materials. Reported slope values correspond to the exponents of asymptotic power law relationships between either τ and E^*, or Ψ_L and E^*.

for cases with very low K values. Intermediate Ψ_L values (0.1–1) correspond to a transitional regime, with a drastic modification of the sensitivity of τ with respect to U and K. All investigated settings display $\Psi_L > 1$, expect the Southeastern Australian Escarpment (A1 and A2), and thus their dynamics involve significant nonlinear contributions to the hillslope sediment flux, with response times ranging from 10 ka (OR and GM) to several 100s of ka.

Very low uplift rates (<1 m/Ma) imply a near-linear response and $\tau \propto K^{-1}$ (Figure 2a), except for cases with very low transport coefficients. In this regime, the more efficient the sediment transport is to begin with, the faster a hillslope will react to perturbations, all else being equal. On the other hand, for high uplift rates (>1,000 m/Ma) and dominantly nonlinear behavior, τ increases as K^{B-1} over all the range of reported transport coefficient values (Richardson et al., 2019). This may seem counter-intuitive at first, but it reflects the fact that greater intrinsic transport efficiency also implies a less steep hillslope that is farther below its threshold gradient (in a sense, it gets less extra help from gravity). Intermediate U values (1–100 m/Ma) are characterized by a non-monotonic evolution, with a maximum τ value at the transition between the linear and nonlinear regimes (Figure 2a).

There is significant overlap between the arid (AI < 0.5) and humid (AI > 0.5) subsets in the transport coefficient database of Richardson et al. (2019), with very close modal values (Figure 2a). But arid climates' K distribution is skewed toward lower values, with some cases displaying K an order of magnitude lower than the mode of the whole data set. In the nonlinear regime, for a given U, decreasing K by an order of magnitude will yield a similar change in the response time. Conversely, for a given K, an order of magnitude change in U triggers a nearly 100-fold change in the response time. Despite having their K and U spread over

almost two orders of magnitude, most investigated case studies are close to the transition between the linear and nonlinear regimes corresponding to the local τ maximum, with the exception of OR, which presents the maximum Ψ_L value in our data set and is clearly in the nonlinear regime.

We show here that E^* and Ψ_L are related through Equation 14, with two distinct regimes (Figure 2b). The first is a purely linear-diffusive regime, with $\Psi_L \ll 1$, $E^* \ll 1$, and $\Psi_L \propto E^{*2}$. The second is a nonlinear regime, for $\Psi_L \gg 1$ and $E^* \gg 1$. Here, the rate of increase in Ψ_L with respect to E^* is less rapid, with $\Psi_L \propto E^*$. For a given K, response time is constant for low E^* hillslopes, consistently with linear diffusion theory, and it decreases very rapidly with increasing E^*, as $\tau \propto E^{*-B}$, when moving into the nonlinear domain (dashed brown lines on Figure 2b). For a given baselevel fall (uplift) rate U (solid brown lines on Figure 2b), the evolution of τ is non-monotonic, as already observed on Figure 2a. In the linear diffusion regime, τ increases as E^* and then $\tau \propto E^{*1-B}$ for hillslopes dominated by nonlinear sediment fluxes. Over the range of U considered here, a local maximum appears at $E^* \sim 2$, coincident with the change in scaling between E^* and Ψ_L, for Ψ_L between 0.1 and 1.

We again observe that the investigated case studies are close to the transition zone between the two regimes, but mostly on the nonlinear side of that transition, with the exception of the Southeastern Australian Escarpment (A1 and A2). An increase in U or a decrease in K would tip them further in the nonlinear domain, with a drop in their response time τ. Conversely, a decrease in U or an increase in K would bring them closer to the transition, but with only a limited influence on τ.

3.2. Response to Oscillatory Forcing

Here we analyze hillslope response to oscillating TD (K oscillations) or BU (U oscillations) forcing (Equation 5). We quantify the response gain G, as the ratio between the normalized amplitudes of the output (sediment flux) and input (forcing) signals:

$$G = \frac{\Delta F / F_{ss}}{2a}, \tag{15}$$

where ΔF is the peak-to-peak amplitude of the sediment flux response, F_{ss} is the steady state flux, used for normalization of the output signal, and $2a$ is the peak-to-peak amplitude factor of the input forcing (Equation 5 and Figures S1 and S2). Gain represents the strength of the response relative to that of forcing. A one-to-one relationship between forcing and response would correspond to $G = 1$; if $G < 1$ the response is damped, and if $G > 1$ it is amplified.

For BU (U) fluctuations, we observe that gain is near zero at high frequencies and moves toward 1 at low frequencies, whereas the evolution is the opposite in the TD (K) case (Figure 3).

Short-term fluctuations in K instantaneously modulate the sediment flux without time for morphological adjustment of the hillslope. On the other hand, longer timescale variations in K are slow enough to allow the hillslope to adjust its morphology and remain close to steady state, with a constant sediment flux matching the constant uplift rate and a gain close to 0.

In the BU case, high-frequency oscillations in U are too fast to be propagated upslope and remain a very local effect at the base of the hillslope, which does not induce a global response. High-frequency U oscillations therefore yield a gain close to 0. On the other hand, if the forcing period is longer than the hillslope response time, upslope propagation can trigger a global response in terms of sediment flux variation.

Overall, decreasing K (Figure 3a, dotted curves) or increasing U (Figure 3b, dashed curves) by a factor of 10 with respect to the reference model moves the hillslope toward the nonlinear regime, with a strong decrease in the response time. For both types of forcing a decrease in K (Figure 3a, dotted curves) leads to an earlier transition when increasing the forcing period due to the corresponding shorter response time (indicated by the dotted vertical lines on Figure 3).

Interestingly, increasing K by a factor 10 (Figure 3a, dashed curves) does not substantially change the response curves (for either type of forcing), which is consistent with the similar response times for the reference and $K \times 10$ models (solid and dashed vertical lines respectively on Figure 3). The response time in the

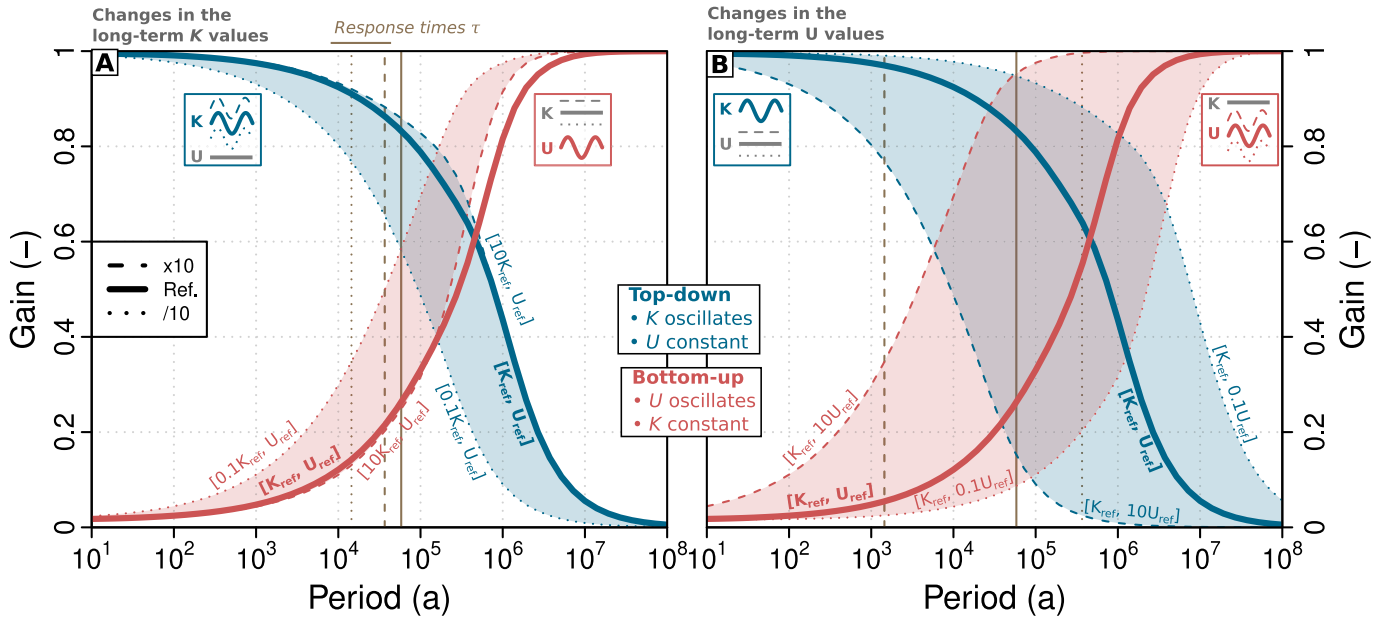

Figure 3. Sensitivity of hillslope sediment flux to oscillation period for Top-Down (TD) (K oscillations, blue) and Bottom-Up (BU) (U oscillations, red) forcing. The response curves show the evolution of gain, defined as the ratio of the output to input signals normalized amplitudes (Equation 15), as a function of the input forcing period. Examples of corresponding time-series are presented on Figures S1 and S2. Thick solid lines correspond to reference values for both U and K (100 m/Ma and 0.01 m^2/a, respectively, Table S1). Dashed and doted lines corresponds to U_{ref} or K_{ref} ×10 or ×0.1, respectively. See Figure 1 for the location of the different combinations in the (U;K) plane. Vertical lines (solid, dashed, and dotted) indicate the response times (τ) for the corresponding hillslopes (Equation 13). (a) Long-term erosion rate is fixed to the reference value U = 100 m/Ma (but fluctuates around this value in the BU cases). Three values of K are tested (reference, ×10, ×0.1), which in the TD cases (K oscillations) correspond to the average value. (b) Long-term transport coefficient is fixed to the reference value K = 0.01 m^2/a (but fluctuates around this value in the TD cases). Three values of U are tested (reference, ×10, ×0.1), which in the BU cases (U oscillations) correspond to the average value.

$K \times 10$ model is actually slightly shorter than the reference case (Figures 1 and 2a), as the evolution of τ is non-monotonic, with a maximum in response time at the transition between the linear and nonlinear regimes; the reference and $K \times 10$ cases are located on both sides of this transition, and have relatively similar response times.

Changes in the background uplift rate (Figure 3b) are similarly shifting the response to the variations in the forcing period, consistently with the effect of U on the response time of the hillslope (Figure 1). The amplitude of this shift appears to be larger than what is induced by the variations in K (Figure 3a).

We now consider response curves to TD forcing (time variations in K) using reference values of K from the observations compiled by Richardson et al. (2019) (Figure 4a). In order to further analyze the role of climatic context, we first use mean K values for the whole data set, and then for arid (AI < 0.5) and humid subsets (solid lines on Figure 4a). Due to the considerable overlap between the distributions, the response curves are very similar. We also test the response for the lowest quartile Q_1 of the arid subset (AI < 0.5) and the highest quartile Q_3 of the humid subset (AI > 0.5). In this case, the two climatically contrasting settings yield distinct response curves, with gain differences up to 0.2 for a given forcing frequency.

We can also analyze the impact of changes in the climatic forcing frequency, such as the shift occurring at the Mid-Pleistocene Transition (MPT), when the dominant period of oscillations, as recorded by marine oxygen isotopes, shifted from the orbital obliquity period (40 ka) to the eccentricity period (100 ka), at ~800 ka ago. In the case of TD forcing, such shift in frequency would induce a decrease in response gain. For high-K or low-U settings, where linear diffusion is prevalent, this decrease in gain is <0.1, but can be >0.2 for high-U or low-K situations, when the hillslope behavior is dominated by nonlinear processes.

Finally, we calculate the response curves to TD forcing using the parameters compiled for the investigated case studies (Table S2 and Figure 4b). We observe the whole range of responses for this selection of sites, with areas such as the Southeastern Australian Escarpment (A1 and A2) showing high gain, with only a slight decrease over the full range of periods. On the other hand, in settings such as the Gabilan Mesa (GM)

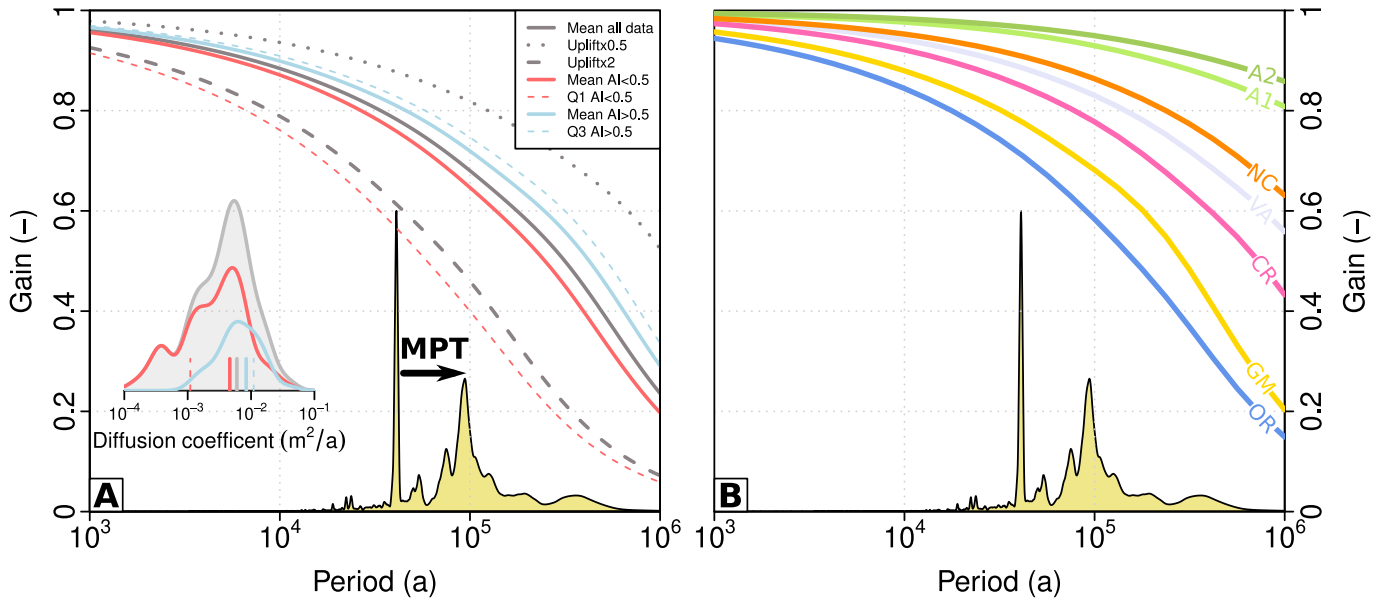

Figure 4. (a) Response curves for Top-Down (TD) forcing (Figure 3), where the transport coefficient is set to the average values of Richardson et al. (2019) data set. Dark gray is for all data ($\bar{K}$ =59.8 cm^2/a), whereas red and blue lines correspond to Aridity Index (AI) lower ($\bar{K}$ =46.2 cm^2/a) or higher ($\bar{K}$ =83.9 cm^2/a) than 0.5, respectively. Dashed red and blue lines correspond to first quartile for AI < 0.5 and third quartile for AI > 0.5, respectively. Reference uplift rate value is 100 mm/ka, and other parameters are from Table S1. Dashed and dotted gray lines correspond to reference uplift rate multiplied by factors 2 and 0.5, respectively. Yellow curve is the power spectrum density from Lisiecki and Raymo (2005) δ^{18}O stack (arbitrary units). Black arrow denotes the shift in dominant climatic oscillation period at the Mid-Pleistocene Transition (MPT, 40–100 ka). (b) Response curves for TD forcing with hillslopes parameters set to the cases studies used here (Table S2). References to labels and colors are the same as Figure 1.

or the Oregon Coast Range (OR) gain decreases from ~0.9, down to <0.2 when increasing the forcing period. When considering the MPT, the frequency shift alone would imply a decrease of ~0.2 for the response gain. Overall, the sensitivity of hillslope response to the frequency content of climatic fluctuations appears to be quite different among these different locations.

4. Discussion and Conclusions

Our results illustrate a complex hillslope response to various types of forcing, which is controlled by the transition between linear and nonlinear regimes (Roering et al., 2001). The various combinations of transport coefficient K and relative uplift rate U at the foot of the hillslope set its Ψ_L value and have a complex influence on its dynamics (Figure 1). Parameters describing the morphology of the hillslope, such as nondimensional erosion rate E^* (Equation 8), can be expressed as functions of the U/K ratio, such that changing U and K by the same factor does not impact steady state hillslope morphology. Conversely the hillslope response time τ (Equation 13) can not be expressed as a function of the U/K ratio, which implies that a given hillslope morphology, as defined by E^* value, can correspond to very different response times. These contrasts can reach almost one order of magnitude, depending on the individual U and K values, as illustrated by the differences in τ despite similar E^* in the VA versus GM or CR versus NC case studies (Figure 2b).

For hillslopes eroding in the 10–100 m/Ma range, the mode of K values from the Richardson et al. (2019) data set is almost coincident with the local maxima for τ (Figure 2a), implying that moderate climate-driven changes in K will have only a modest impact on the value of τ. The trade-off between U and K in controlling Ψ_L and E^* values is reflected in the position of the local maximum in τ, which occurs at higher K values when U increases. In the nonlinear dominated domain, changing U by an order of magnitude implies a nearly two order of magnitude change in τ, whereas a similar amplitude change in K results only in less than an order of magnitude change in τ (Figure 2a). This importance of changes in U on hillslope response is confirmed by the steep slope of the constant-K curves from Figure 2b (dashed brown lines) for $E^* > 1$, as well as by the different impacts on the response curves of orders of magnitude changes in background K and U (Figure 3a vs. Figure 3b).

The filtering or transmitting behavior of hillslopes with respect to high frequency environmental perturbations depends the values of U and K, as well as on the type of forcing, as TD and BU forcing are buffered at the opposite ends of the spectrum (Figure 3). For the usual range of K values, hillslopes transmit TD forcing up to period of ~100 ka (gain G close to 1), but with a significant lowering of this limit when increasing uplift rates (Figure 3b, blue dashed curve). As a consequence, the sediment flux from near-threshold hillslopes in high-uplift regions appears less likely to be directly modulated by climate over the 10–100 ka range of astronomical forcing frequencies. On the other hand, BU forcing are strongly filtered at short periods (G close to 0) (Furbish & Fagherazzi, 2001). Climatic fluctuations can of course act simultaneously as TD and BU-types forcing. Simultaneous changes in vegetation, soil moisture, and runoff generation can potentially lead to complex (but spatially synchronous) modulation of K in the frame of a TD-type forcing (e.g., Bovy et al., 2016). The case of vegetation changes when shifting toward drier or wetter climates is known to trigger complex responses across landscapes. Such responses mean that K is not necessarily a simple linear function of mean annual precipitation. For example, transport efficiency may actually increase when a dense and thick forest is replaced with shrubs or grass under a more arid climate (Pelletier, 2014; Pelletier et al., 2016; Sharma et al., 2021). Climate changes can also modulate river incision efficiency at the foot of the hillslope as a BU-type forcing, which acts locally and then propagates upslope with progressive adjustments. In our simulations, we have separated the two types of forcing in order to isolate their specific properties (Figure 3). In many settings, it is likely that climatic fluctuations might trigger both types of responses, acting simultaneously on the hillslope, with potential constructive or destructive interactions, depending on the amount of phase offset between the two signals. However, orbitally controlled climatic forcing operating in the 10–100 ka range is expected to have a limited expression on river profiles (Goren, 2016), which is an additional argument for a limited impact of astronomically tuned BU-type forcing on hillslopes.

The response curves for TD-type forcing (Figure 4) show a steep decline over the 10 ka to 1 Ma range, implying that the 40 to 100 ka shift associated with the Mid-Pleistocene Transition (MPT) could have triggered a drop in gain up to 0.2 for arid and/or rapidly eroding (i.e., high E^*) landscapes, whereas for wetter or more slowly eroding landscapes (i.e., low E^*) the drop is limited to <0.1. Overall, a frequency decrease such as the MPT resulted in a significant lowering of the sensitivity of hillslopes to climatically driven oscillations in transport coefficient. The pure frequency shifts considered here are likely to be superimposed on climatically controlled increases or decreases in the long-term average transport coefficient value, resulting in a corresponding transient perturbation of the averaged sediment flux.

For TD forcing at glacial-interglacial frequencies, the expected gain ranges from about 0.4 to 0.9 (Figure 4a). To understand how this translates into variations in hillslope sediment supply, one needs estimates of the amplitude of climatically modulated variations in K. An analysis of frost-driven creep by Anderson et al. (2013) presented an example in which variations in mean annual temperature similar to those associated with ice-age cycles produced variation in K between 0.005 and 0.04 m^2/y. If one treated this as a sinusoidal variation around the mid-point, the corresponding amplitude would be about ±0.8 times the mean. Given the above range of gain values, this translates into an amplitude of sediment flux variation between 0.3 and 0.7 times the temporal mean.

Conversely, given data on climatically controlled variations in hillslope sediment flux, one could also infer the corresponding variation in K. For example, Hughes et al. (2009) documented a near-doubling increase in flux (0.0012–0.0022 m^2/y) in New Zealand associated with vegetation change across the Pleistocene-Holocene transition. If this were treated as sinusoidal oscillations about the midpoint, a flux variation amplitude of about ±0.3 times the mean with a gain range of 0.4–0.9 implies an amplitude of flux variation between about 33% and 74% of the mean flux. This kind of information is valuable for understanding and modeling whole-landscape response to cyclic climate forcing (e.g., Langston & Tucker, 2018).

Globally, our results illustrate a complex and frequency-dependent hillslope response to oscillating boundary conditions. The linear/nonlinear transition implies the potential for complex non-monotonic evolution and a sensitivity to changes in periodicity over Milankovitch time scales, such as the 40 to 100 ka Mid-Pleistocene Transition. As most sediment production occurs on hillslopes, global-scale analysis of the impact of climate fluctuations on landscapes should integrate the intrinsic hillslope responses to various types of forcing.

Acknowledgments
This research was supported by an IUF fellowship and ANR grant TopoExtreme to VG and NSF grant EAR-1831623 to GT. The authors thank two anonymous reviewers for their help in improving our manuscript.

Data Availability Statement

Data used in this study are available through Codilean et al. (2018), Godard et al. (2019, 2020), Grieve et al. (2016), Hurst et al. (2012), Richardson et al. (2019), and Roering et al. (2007).

References

Anderson, R. S., Anderson, S. P., & Tucker, G. E. (2013). Rock damage and regolith transport by frost: An example of climate modulation of the geomorphology of the critical zone. *Earth Surface Processes and Landforms*, *38*(3), 299–316. https://doi.org/10.1002/esp.3330

Andrews, D. J., & Bucknam, R. C. (1987). Fitting degradation of shoreline scarps by a nonlinear diffusion model. *Journal of Geophysical Research*, *92*(B12), 12857–12867. https://doi.org/10.1029/jb092ib12p12857

Bovy, B., Braun, J., & Demoulin, A. (2016). A new numerical framework for simulating the control of weather and climate on the evolution of soil-mantled hillslopes. *Geomorphology*, *263*, 99–112. https://doi.org/10.1016/j.geomorph.2016.03.016

Braun, J., Voisin, C., Gourlan, A. T., & Chauvel, C. (2015). Erosional response of an actively uplifting mountain belt to cyclic rainfall variations. *Earth Surface Dynamics*, *3*(1), 1–14. https://doi.org/10.5194/esurf-3-1-2015

Clubb, F. J., Mudd, S. M., Hurst, M. D., & Grieve, S. W. (2020). Differences in channel and hillslope geometry record a migrating uplift wave at the Mendocino triple junction, California, USA. *Geology*, *48*(2), 184–188. https://doi.org/10.1130/g46939.1

Codilean, A. T., Munack, H., Cohen, T. J., Saktura, W. M., Gray, A., & Mudd, S. M. (2018). OCTOPUS: An open cosmogenic isotope and luminescence database. *Earth System Science Data*, *10*(4), 2123–2139. https://doi.org/10.5194/essd-10-2123-2018

Culling, W. E. H. (1960). Analytical theory of erosion. *The Journal of Geology*, *68*(3), 336–344. https://doi.org/10.1086/626663

Dietrich, W. E., Bellugi, D. G., Sklar, L. S., Stock, J. D., Heimsath, A. M., & Roering, J. J. (2003). Geomorphic transport laws for predicting landscape form and dynamics. In P. R. Wilcock, & R. M. Iverson (Eds.), Prediction in geomorphology (Geophysical Monograph Series, Vol. 135, pp. 103–132). American Geophysical Union.

Doane, T. H., Furbish, D. J., Roering, J. J., Schumer, R., & Morgan, D. J. (2018). Nonlocal sediment transport on steep lateral moraines, eastern Sierra Nevada, California, USA. *Journal of Geophysical Research: Earth Surface*, *123*(1), 187–208. https://doi.org/10.1002/2017jf004325

Fernandes, N. F. N., & Dietrich, W. W. E. (1997). Hillslope evolution by diffusive processes: The timescale for equilibrium adjustments. *Water Resources Research*, *33*(6), 1307–1318. https://doi.org/10.1029/97wr00534

Furbish, D. J., & Fagherazzi, S. (2001). Stability of creeping soil and implications for hillslope evolution. *Water Resources Research*, *37*(10), 2607–2618. https://doi.org/10.1029/2001wr000239

Furbish, D. J., & Roering, J. J. (2013). Sediment disentrainment and the concept of local versus nonlocal transport on hillslopes. *Journal of Geophysical Research: Earth Surface*, *118*(2), 937–952. https://doi.org/10.1002/jgrf.20071

Gilbert, G. K. (1909). The convexity of hilltops. *The Journal of Geology*, *17*(4), 344–350. https://doi.org/10.1086/621620

Godard, V., Dosseto, A., Fleury, J., Bellier, O., Siame, L., & ASTER, T. (2019). Transient landscape dynamics across the Southeastern Australian Escarpment. *Earth and Planetary Science Letters*, *506*, 397–406. https://doi.org/10.1016/j.epsl.2018.11.017

Godard, V., Hippolyte, J.-C., Cushing, E., Espurt, N., Fleury, J., Bellier, O., & Ollivier, V. (2020). Hillslope denudation and morphologic response to a rock uplift gradient. *Earth Surface Dynamics*, *8*(2), 221–243. https://doi.org/10.5194/esurf-8-221-2020

Godard, V., Tucker, G. E., Fisher, G. B., Burbank, D. W., Bookhagen, B., Burch Fisher, G., et al. (2013). Frequency-dependent landscape response to climatic forcing. *Geophysical Research Letters*, *40*(5), 859–863. https://doi.org/10.1002/grl.50253

Goren, L. (2016). A theoretical model for fluvial channel response time during time-dependent climatic and tectonic forcing and its inverse applications. *Geophysical Research Letters*, *43*(20), 10753–10763. https://doi.org/10.1002/2016gl070451

Grieve, S. W. D., Mudd, S. M., Hurst, M. D., & Milodowski, D. T. (2016). A nondimensional framework for exploring the relief structure of landscapes. *Earth Surface Dynamics*, *4*(2), 309–325. https://doi.org/10.5194/esurf-4-309-2016

Hughes, M. W., Almond, P. C., & Roering, J. J. (2009). Increased sediment transport via bioturbation at the last glacial-interglacial transition. *Geology*, *37*(10), 919–922. https://doi.org/10.1130/g30159a.1

Hurst, M. D., Mudd, S. M., Walcott, R., Attal, M., & Yoo, K. (2012). Using hilltop curvature to derive the spatial distribution of erosion rates. *Journal of Geophysical Research*, *117*(F2), F02017. https://doi.org/10.1029/2011jf002057

Langston, A. L., & Tucker, G. E. (2018). Developing and exploring a theory for the lateral erosion of bedrock channels for use in landscape evolution models. *Earth Surface Dynamics*, *6*(1), 1–27. https://doi.org/10.5194/esurf-6-1-2018

Langston, A. L., Tucker, G. E., & Anderson, R. S. (2015). Interpreting climate-modulated processes of terrace development along the Colorado Front Range using a landscape evolution model. *Journal of Geophysical Research: Earth Surface*, *120*(10), 2121–2138. https://doi.org/10.1002/2014jf003403

Lisiecki, L. E., & Raymo, M. E. (2005). A Pliocene-Pleistocene stack of 57 globally distributed benthic $d^{18}O$ records. *Paleoceanography*, *20*(1), PA1003. https://doi.org/10.1029/2004pa001071

Mudd, S. M. (2016). Detection of transience in eroding landscapes. *Earth Surface Processes and Landforms*, *42*(1), 24–41. https://doi.org/10.1002/esp.3923

Ouimet, W. B., Whipple, K. X., & Granger, D. E. (2009). Beyond threshold hillslopes: Channel adjustment to base-level fall in tectonically active mountain ranges. *Geology*, *37*(7), 579–582. https://doi.org/10.1130/g30013a.1

Pelletier, J. D. (2014). The linkages among hillslope-vegetation changes, elevation, and the timing of late-Quaternary fluvial-system aggradation in the Mojave Desert revisited. *Earth Surface Dynamics*, *2*(2), 455–468. https://doi.org/10.5194/esurf-2-455-2014

Pelletier, J. D., Nichols, M. H., & Nearing, M. A. (2016). The influence of Holocene vegetation changes on topography and erosion rates: A case study at Walnut Gulch Experimental Watershed, Arizona. *Earth Surface Dynamics*, *4*, 471–488. https://doi.org/10.5194/esurf-4-471-2016

Perron, J. T. (2011). Numerical methods for nonlinear hillslope transport laws. *Journal of Geophysical Research*, *116*(F2), F02021. https://doi.org/10.1029/2010jf001801

Richardson, P. W., Perron, J. T., & Schurr, N. D. (2019). Influences of climate and life on hillslope sediment transport. *Geology*, *47*(5), 1–4. https://doi.org/10.1130/g45305.1

Roering, J. J., Kirchner, J. W., & Dietrich, W. E. (1999). Evidence for nonlinear, diffusive sediment transport on hillslopes and implications for landscape morphology. *Water Resources Research*, *35*(3), 853–870. https://doi.org/10.1029/1998wr900090

Roering, J. J., Kirchner, J. W., & Dietrich, W. E. (2001). Hillslope evolution by nonlinear, slope-dependent transport: Steady state morphology and equilibrium adjustment timescales. *Journal of Geophysical Research*, *106*(B8), 16499–16513. https://doi.org/10.1029/2001jb000323

Roering, J. J., Perron, J. T., & Kirchner, J. W. (2007). Functional relationships between denudation and hillslope form and relief. *Earth and Planetary Science Letters*, *264*(1–2), 245–258. https://doi.org/10.1016/j.epsl.2007.09.035

Romans, B. W., Castelltort, S., Covault, J. A., Fildani, A., & Walsh, J. (2016). Environmental signal propagation in sedimentary systems across timescales. *Earth-Science Reviews*, *153*, 7–29. https://doi.org/10.1016/j.earscirev.2015.07.012

Sharma, H., Ehlers, T. A., Glotzbach, C., Schmid, M., & Tielbörger, K. (2021). Effect of rock uplift and Milankovitch timescale variations in precipitation and vegetation cover on catchment erosion rates. *Earth Surface Dynamics*, *9*(4), 1045–1072.

Simpson, G., & Castelltort, S. (2012). Model shows that rivers transmit high-frequency climate cycles to the sedimentary record. *Geology*, *40*(12), 1131–1134. https://doi.org/10.1130/g33451.1

Tucker, G. E., & Bradley, D. N. (2010). Trouble with diffusion: Reassessing hillslope erosion laws with a particle-based model. *Journal of Geophysical Research*, *115*, 1–12. https://doi.org/10.1029/2009jf001264

Watkins, S. E., Whittaker, A. C., Bell, R. E., McNeill, L. C., Gawthorpe, R. L., Brooke, S. A., & Nixon, C. W. (2018). Are landscapes buffered to high-frequency climate change? A comparison of sediment fluxes and depositional volumes in the Corinth Rift, central Greece, over the past 130 k.y. *GSA Bulletin*, *131*(3–4), 372–388. https://doi.org/10.1130/b31953.1